Racial Differences in 3-D Nuclear Chromatin Patterns of Prostate Cancer

André Huisman[1], Lennert S. Ploeger[1], Hub F.J. Dullens[1], Jeroen A.M. Belien[2], Gerrit A Meijer[2], Neal Poulin[1], William E. Grizzle[3] and Paul J. van Diest[1,*]

[1]*Department of Pathology, University Medical Center, Utrecht;* [2]*Department of Pathology, VU University Medical Center, Amsterdam, The Netherlands and* [3]*Department of Pathology, University of Alabama at Birmingham, Alabama, USA*

Abstract: *Purpose*: There is a significant difference in prostate cancer incidence and stage corrected mortality between African-American (AA) and Caucasian-American (CA) men. These differences have largely been contributed to social-economic factors, yet variation in prostate cancer related gene expression has been found as well. The aim of this study was to analyze whether these differences are reflected also in the 3-D distribution patterns of the nuclear chromatin.

Materials and Methods: Prostatectomy sections from 21 prostate cancer patients (10 AA and 11 CA) were cut and nuclear DNA was stained with TO-PRO-3. 3-D image stacks of selected malignant areas were obtained by confocal laser scanning microscopy. Image analysis was performed using in-house developed software for 3-D semi-automated segmentation and computation of DNA content and our previously developed 3-D nuclear texture features. The power of these features to discriminate between AA and CA patients was established by univariate ROC and linear discriminant analyses, stratifying for prognosis.

Results: Five 3-D texture features discriminated between AA and CA men irrespective of prognosis, 27 features had discriminative value for AA and CA men in the subgroup of bad prognosis patients, and 8 features in the good prognosis subgroup. Several features had additional discriminative value in multivariate discriminant analysis.

Conclusions: There are differences in the 3-D nuclear chromatin distribution between AA and CA men with similar prognosis. This is further evidence that the differences of prostate cancer in AA and CA men are not only related to socioeconomic differences, but also to genomic differences.

Key Words: Confocal laser scanning microscopy, 3-D nuclear texture, image analysis, prostate cancer, racial differences.

INTRODUCTION

There is a significant difference in prostate cancer incidence and mortality between African-American (AA) and Caucasian American (CA) men. Death rates from prostate cancer among AA men are more than twice the rates in CA men, even when diagnosed at the same clinical stage [1]. AA men having prostate cancer generally show higher PSA blood levels at a younger age and more extensive disease[2-4]. These differences have usually been associated with differences in social-economic environment [5]. However, it remains controversial if the higher mortality rates in AA men are explained only by these differences, because molecular differences have been found as well [6]. It is known that there are racial differences in serum vitamin D levels, which is associated with a higher risk for several diseases, among which is also prostate cancer [7]. On the genetic level for example, a higher frequency of mutations in the EphB2 gene was found in tumors from AA patients compared to tumors from CA men [8]. Another study showed that the epidermal growth factor receptor gene, known to be of importance in the oncogenesis of prostate cancer [9], is significantly more often overexpressed in AA patients [10].

These genomic differences are reflected in morphological differences, used by pathologists in daily practice to diagnose malignancy, like increased nuclear size, presence of and increased size of nucleoli and aberrant chromatin distribution patterns [11-13]. The nuclear chromatin distribution in genetically altered cells is generally coarsely-clumped with multiple chromacenters and larger nucleoli, as opposed to finely granular with few chromacenters and no or small nucleoli in normal cells. These changes are often rather subtle or even subvisible, and are referred to as "malignancy associated changes" as they may be detected in morphologically benign cells as well [13-15]. They are therefore best not visually assessed but mathematically quantified by computerized image analysis as "texture features" that are very sensitive and not prone to observer subjectivity.

A number of papers have been published on the clinical value of the assessment of DNA content and nuclear texture features by image analysis, using conventional 3-4μm thick prostate tissue sections has been produced [16-18]. However, imaging thin tissue slices obviously may result in loss of valuable 3-D texture information. This can be avoided by preparing cytospins from cell suspensions, but this introduces artifacts by the flattening of nuclei while spinning them down. Furthermore, the morphological context of the analyzed nuclei is completely lost.

*Address correspondence to this author at the Department of Pathology, University Medical Center Utrecht, PO Box 85500, 3508 GA Utrecht, The Netherlands; Tel: (31) 30 2506565; Fax: (31) 30 2544990;
E-mail p.j.vandiest@umcutrecht.nl

These drawbacks can be completely avoided by imaging thick sections (typical 10-50 μm) by Confocal Laser Scanning Microscopy (CLSM). Thin optical slices are acquired at high resolution by confocal imaging, and these are subsequently reconstructed in 3-D [19]. In previous studies we described 3-D segmentation procedures to obtain individual nuclei from an acquired image stack [20], established the required nuclear sample size to achieve proper 3-D DNA histogram quality [21], developed an optimal tissue processing technique for 3-D Confocal Laser Scanning Microscopy (CLSM) [22], described the successful software implementation of 3-D nuclear texture features [23] and performed a pilot study on the clinical value of the assessment of DNA content and nuclear texture features by CLSM [13]. The aim of the present study was to analyze whether the racial differences in clinical presentation and genomics between prostate cancer in AA and CA men are reflected in the 3-D distribution patterns of nuclear chromatin in prostate cancer cells.

MATERIALS AND METHODS

Tissue Preparation

Prostatectomy tissue sections from 10 AA men and 11 CA men having prostate cancer were selected by a pathologist (WEG) from the archives of the Department of Pathology, University of Alabama at Birmingham, USA. Twelve of these patients had a good prognosis (AA n=8, CA n=4) and 9 had a bad prognosis (AA n=2, CA n=7). The patients included in this study were approximately matched on age (range: 50-71 years, average 63 years, standard deviation: 6 years), stage and Gleason score (Table **1**).

Table 1.   Distribution of Gleason Scores and Stage Among the African-American (AA) and Caucasian American (CA) Patients Studied

	AA		CA	
	Good	**Bad**	**Good**	**Bad**
Gleason 6-7	8	1	3	6
Gleason 8-10		1		
Gleason unknown			1	1
Stage T2	5		3	
Stage T3	3	2	1	5
Stage Unknown				2

Fourteen micron thick sections were cut from representative paraffin-embedded tissue blocks. Our previously developed protocol [22] was used for staining: incubation with RNase-A for 1 hour and staining with TO-PRO-3 (Molecular Probes, Eugene, OR, USA) in a concentration of 1:2,200 for 2 hours at room temperature [24]. After rinsing with distilled water the samples were mounted in Vectashield (Vector Laboratories, Burlingame, CA, USA). The coverslip was sealed with nail polish.

Image Acquisition and Analysis

Image stacks were acquired with a confocal microscope (TCS SP2 AOBS, Leica Microsystems, Heidelberg, Ger-

many) using the ×40/1.25 NA oil immersion objective with a zoom factor of 2.0 (total magnification of ×80). To obtain measurements for at least 300 nuclei as previously established [21], between the 10 and 15 image stacks were acquired, depending on the number of nuclei per image stack. The different microscopic fields were selected approximately 3.0 mm apart from each other to avoid potential bleaching of neighboring fields during image acquisition. The x-y coordinates of each field were stored using in-house developed add-on software for the confocal microscope [13]. These coordinates were used for automated acquisition of the defined fields. Subsequently, the bottom and top of the defined fields were identified interactively as the slices where hardly any signal was detectable [20]. Stacks of approximately 120 2-D digital images (512x512 pixels) were obtained, depending on the effective thickness of the tissue. Resolution at the specimen level was 0.292x0.292x0.285 μm^3 and the dynamic range was 12 bits.

The image stacks were segmented to obtain the boundaries for the individual nuclei. These nuclei were analyzed off-line using in-house developed software, as described previously [21]. Segmentation was stopped when 300 nuclei were collected.

Texture Feature Computation

Our in-house developed software for the computation of 35, 3-D texture features was used as described previously [23]. In short, the selected texture features are from three different classes: discrete features, Markovian features and fractal features. General descriptive statistical features of the grey-value distribution were computed as well [25]. Discrete texture features summarize several general statistics for the different chromatin condensation states in the nucleus, corresponding to different ranges of grey-values. The Markovian features involve second order grey level statistics and are computed from co-occurrence matrices, representing the joint probability that pairs of grey-level combinations co-occur together. Several statistics can be computed from those matrices: heuristic features, statistical features and features taken from information theory [26]. Fractals are mathematical objects which have similar details on every scale. Fractals have a strong correlation with human judgment of texture roughness [27]. Fractal texture features are used to describe the fractal properties of the nuclei.

Data Analysis

First, Receiver Operating Characteristic (ROC) curves were plotted for each feature as a graphical representation of the trade off between the false negative and false positive rates, and the area under curve (AUC) was calculated as a measure of discriminative power. ROC computation was performed for the complete dataset (AA versus CA men) as well as on the nuclei grouped by prognosis group (AA good versus CA good; AA bad versus CA bad). Discriminative texture features had an AUC of 0.5-1, and features with an AUC ≥ 0.70 were arbitrarily considered to have good discriminative power.

Further, multivariate linear discriminant analysis with step-wise addition of new variables was applied, minimizing Wilks' lambda statistic. Leave-one-out was used as cross validation technique. The five most discriminative texture

features were selected according to the steepest descent in Wilks' lambda statistic. This approach was used to discriminate between the pooled AA and CA nuclei as well as between the pooled AA and CA nuclei within the good and bad prognosis subgroups. Finally, the pooled nuclei of good and bad prognosis patients were discriminated, irrespective of race.

RESULTS

The number of patients per prognosis group and some tumor characteristics are given in Table **1**. The number of segmented nuclei per prognosis group is given in Table **2** for both races. AUC values for the 35 3-D nuclear texture features for discriminating between pooled nuclei from AA men versus CA men are shown in the second column of Table **3**. Five features yielded AUC values above 0.7. The second and third columns show the AUC values after performing an ROC analysis on the pooled nuclei within the subgroups of good and bad prognosis. For the subgroup of patients with bad prognosis, 27 features yielded AUC values above 0.7 when discriminating nuclei from AA and CA men. For the subgroup of patients with good prognosis, 8 features yielded AUC values above 0.7 when discriminating nuclei from AA and CA men. In Fig. (**1**), examples are given of nuclei from AA and CA men of the bad and good prognosis subgroups, showing that also visually there are differences in nuclear texture.

ROC analysis for discriminating between patients having a good and bad prognosis without grouping by race revealed 6 well discriminative features (AUC ≥ 0.70): Grey skewness, Grey kurtosis, Average extinction ratio of low density region, Low versus medium average extinction ratio, Low versus medium high average extinction ratio, and Low versus high average extinction ratio, but none of these had values above 0.8.

In Table **4**, the nuclear texture features that were selected in multivariate linear discriminant analysis are presented, together with the absolute values of their standardized discriminant function coefficients that indicate their relative importance in discriminating between nuclei from AA men and CA men. The discriminant analysis was separately applied on all pooled nuclei of AA and CA men (complete dataset), as well as on the pooled nuclei of AA and CA men of the good and bad prognosis subgroups.

Table **5** shows the performance of the classification functions in terms of the relative amounts of correctly classified nuclei. For the complete dataset, 67% of the nuclei were cor-

rectly identified as being of AA or CA origin. The nuclei from patients having a good prognosis were classified correctly as being from an AA or a CA man in 80% of the cases, and 89% of nuclei from patients having a bad prognosis were classified correctly.
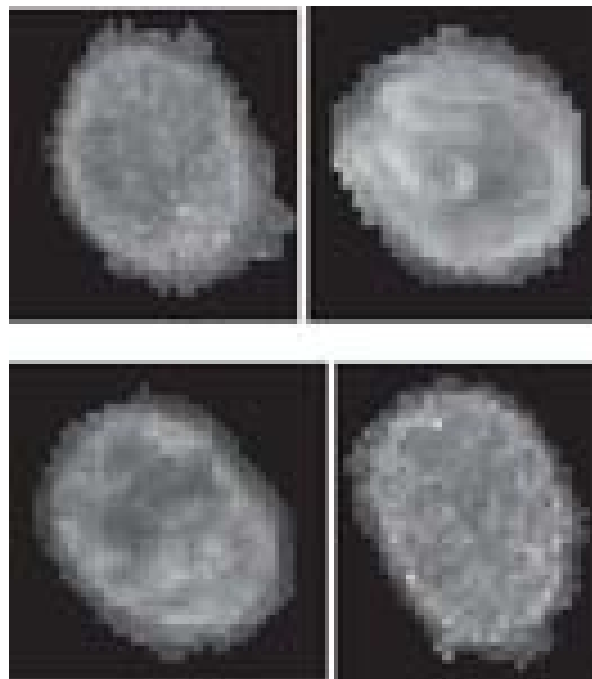

Fig. (1). Examples of maximum intensity projections of nuclei from AA (left) and CA men (right) of the good prognosis (top row) and bad prognosis (bottom row) subgroups, showing that also visually there are differences in nuclear texture. These nuclei are obtained from a stack of prostate tissue stained with TO-PRO-3, acquired by CLSM, imaged with a ×40/1.25 NA oil immersion objective with a zoom factor of 2.0 (total magnification of ×80).

DISCUSSION

The aim of this study was to establish the differences in nuclear chromatin texture between AA and CA patients having prostate cancer. Although technically challenging, we did this in 3-D, as theoretically this should yield more information than conventional 2-D analysis, which we indeed proved in a previous study [23]. Since previous studies showed that 2-D texture have prognostic value in prostate cancer [16, 17], we stratified for prognosis.

In univariate ROC analysis, five 3-D texture features could discriminate well between the nuclear chromatin from

Table 2. Summary of the Number of Segmented Nuclei Per Race and Prognosis Group is Depicted*, as well as the Average Number of Segmented Nuclei Per Image Stack**

Prognosis	AA Men (10 Patients)		CA Men (11 Patients)	
	# Patients	# Nuclei	# Patients	# Nuclei
Good	8	1621*, 180**	4	637*, 159**
Bad	2	307*, 154**	7	1619*, 179**
Totals	10	1928*, 175**	11	2256*, 174**

Table 3.   AUC Values for the 35, 3-D Nuclear Texture Features for Discriminating between Pooled Nuclei from all AA Men and CA Men Independent of Prognosis (Second Column), as well as for the Subgroups with Bad Prognosis (Third Column) and Good Prognosis (Fourth Column). Strongly Discriminating Features (Having an AUC Value Greater than or Equal to 0.7) are Depicted in Bold

Feature Type	All Cases	Subgroup with Bad Prognosis	Subgroup with Good Prognosis
Grey sum	0.56	**0.79**	**0.79**
Grey mean	0.53	0.56	0.67
Grey variance	0.67	**0.72**	0.68
Grey skewness	0.65	**0.76**	0.57
Grey kurtosis	0.61	**0.74**	0.66
Energy	0.65	**0.79**	0.61
Entropy	0.54	0.58	0.60
Inverse difference moment	0.61	**0.92**	0.66
Inertia	0.68	**0.93**	0.53
Correlation	0.57	0.55	0.67
Cluster shade	0.67	**0.71**	0.65
Cluster prominence	0.65	0.66	0.67
Volume (pixels) of low density region	0.51	**0.85**	**0.74**
Volume (pixels) of medium density region	0.52	**0.85**	0.69
Volume (pixels) of highdensity region	0.51	**0.87**	**0.73**
Average extinction ratio of low dens. region	**0.74**	**0.86**	0.56
Average extinction ratio of med. dens. region	0.67	**0.74**	0.65
Average extinction ratio of high dens. region	**0.73**	**0.83**	0.64
Low vs. medium average extinction ratio	**0.77**	**0.89**	0.61
Low vs. med-high average extinction ratio	**0.77**	**0.89**	0.60
Low vs. high average extinction ratio	**0.77**	**0.89**	0.60
Number of unconnected low areas	0.55	**0.79**	**0.71**
Number of unconn. Medium areas	0.51	0.60	0.53
Number of unconn. high areas	0.55	**0.77**	0.68
Low compactnes	0.52	0.53	0.56
Med compactnes	0.52	**0.80**	**0.74**
High compactnes	0.52	0.69	0.69
Low avg. distance to geo-center	0.52	**0.72**	0.57
Med avg. dist. geo-center	0.52	**0.75**	0.54
High avg.dist. geo-center	0.59	**0.85**	0.54
Asymetry of low region w.r.t. to nuclear center	0.60	**0.84**	**0.84**
med asym.nuc.cntr	0.61	**0.83**	**0.79**
high asym. nuc. Cntr	0.60	**0.85**	**0.83**
Lacunarity	0.53	0.59	0.54
Fractal dimension	0.52	**0.84**	0.66
#features having AUC ≥ 0.7	5	27	8

Table 4. Discriminant Function Coefficients of Different 3-D Nuclear Texture Features Selected in Linear Discriminant Analysis Separating Pooled Nuclei from AA and CA Men. The Discriminant Analysis was Applied on the Complete Dataset, as well as on the Subgroups of Nuclei from Bad and Good Prognosis Cases. Coefficients are Standardized Discriminant Coefficients

Complete Dataset		Good Prognosis Cases		Bad Prognosis Cases	
Texture Feature	Coefficient	Texture Feature	Coefficient	Texture Feature	Coefficient
Grey kurtosis	0.50	Grey mean	1.09	Grey sum	1.22
Compactness of low region	0.75	Grey variance	0.81	Inverse difference moment	0.59
Inertia	0.75	Inertia	1.58	Entropy (of co-occurrence matrix)	0.20
Volume of low density area	0.53	Asymmetry w.r.t. nuclear center of high region	0.49	Fractal dimension	0.34

Table 5. Cross Validated Classification Results of the 3-D Nuclear Texture Features Selected in Linear Discriminant Analysis Shown in Table 3. The Discriminant Analysis was Applied on the Complete Dataset, as well as on the Nuclei Grouped by Prognosis. The Percentages Indicate the Relative Amount of Classified Nuclei as being from a Specified Group[*], Given the Actual Group Membership[**]. The Features in Bold Indicate the Percentage of Correctly Classified Nuclei

	Actual Group Membership[**]	Predicted Group Membership[*]		% Correctly Classified
		AA Men (%)	CA Men (%)	
Complete dataset	AA men	**65**	35	67%
	CA men	31	**69**	
Good prognosis cases	AA men	**76**	24	80%
	CA men	18	**82**	
Bad prognosis cases	AA men	**87**	13	89%
	CA men	4	**96**	

AA patients and that of CA patients (Table **3**). These were all from the class of discrete texture features. Being from the same class, these features are to some extent correlated as well; however, when taking prognosis into account, the classification rates improved significantly. This confirms the idea that prognosis is indeed an important stratification factor. For the subgroup of patients with bad prognosis, no fewer than 27 features (from different classes) yielded AUC values above 0.70 when discriminating nuclei from AA and CA men, with many features having AUC values around or above 0.90. For the subgroup of patients with good prognosis, 8 features yielded AUC values above 0.70 when discriminating nuclei from AA and CA men. Therefore, although there are apparently differences in 3-D nuclear chromatin patterns of prostate cancer nuclei from AA and CA men, these differences are most prominent within the subgroup of patients with bad prognoses. Because the differences between AA and CA men having a bad prognosis are the most outstanding, this is an indication that although these patients have a similar prognosis, there are differences in the genomic processes related to the progress of the disease. These differences might account for the high mortality rate of AA men. The actual underlying genetic events that may explain the differences in nuclear chromatin patterns between AA and CA men are not known, but deserve to be

further studied by e.g. correlating data from genomic arrays and microarray expression analysis with nuclear texture features.

It was interesting to note that irrespective of grade, many of the nuclear texture features could discriminate between patients with good and bad prognosis. This implies that our 3-D features may have prognostic value. It will be interesting to evaluate the comparative prognostic value of 2-D and 3-D features in a subsequent study.

Using the current status of our technology we are able to correctly classify a high percentage of nuclei from AA and CA men. The statistical power of this study would increase if more patient samples would be included. A limitation of the current analysis clearly is the number of texture features that was analyzed compared to the number of cases included in the study. Furthermore, improvements can be made increasing the image quality, especially the resolution in the axial direction. Better image quality may also be obtained by deconvolving the images [28] or by using 4-Pi microscopy [29].

In conclusion, this is the first study describing that 3-D nuclear chromatin texture features obtained by quantitative confocal laser scanning microscopy reveal racial differences

between prostate cancer nuclei from AA and CA men stratified for prognosis. This underlines the hypothesis that there are not only socioeconomic but also genomic differences between prostate cancer in AA and CA men.

REFERENCES

[1]   Jemal A, Murray T, Ward E, *et al*. Cancer statistics, 2005. CA Cancer J Clin 2005; 55(1): 10-30.

[2]   Mavropoulos JC, Partin AW, Amling CL, *et al*. Do racial differences in prostate size explain higher serum prostate-specific antigen concentrations among black men? Urology 2007; 69(6): 1138-42.

[3]   Hoffman RM, Gilliland FD, Eley JW, *et al*. Racial and ethnic differences in advanced-stage prostate cancer: the Prostate Cancer Outcomes Study. J Natl Cancer Inst 2001; 93(5): 388-95.

[4]   Li LC, Okino ST, Dahiya R. DNA methylation in prostate cancer. Biochim Biophys Acta 2004; 1704(2): 87-102.

[5]   Jones BA, Liu WL, Araujo AB, *et al*. Explaining the race difference in prostate cancer stage at diagnosis. Cancer Epidemiol Biomarkers Prev 2008; 17(10): 2825-34.

[6]   Peters N, Armstrong K. Racial differences in prostate cancer treatment outcomes: a systematic review. Cancer Nurs 2005; 28(2): 108-18.

[7]   Roff A, Wilson RT. A novel SNP in a vitamin D response element of the CYP24A1 promoter reduces protein binding, transactivation, and gene expression. J Steroid Biochem Mol Biol 2008; 112(1-3): 47-54.

[8]   Kittles RA, Boffoe-Bonnie A, Moses T, *et al*. A common nonsense mutation in EphB2 is associated with prostate cancer risk in African American men with a positive family history. J Med Genet 2005; 43(6): 507-11.

[9]   Ratan HL, Gescher A, Steward WP, Mellon JK. ErbB receptors: possible therapeutic targets in prostate cancer? BJU Int 2003; 92(9): 890-5.

[10]   Shuch B, Mikhail M, Satagopan J, *et al*. Racial disparity of epidermal growth factor receptor expression in prostate cancer. J Clin Oncol 2004; 22(23): 4725-9.

[11]   Veltri RW, Partin AW, Miller MC. Quantitative nuclear grade (QNG): a new image analysis-based biomarker of clinically relevant nuclear structure alterations. J Cell Biochem Suppl 2000; (Suppl) 35: 151-7.

[12]   Guillaud M, Doudkine A, Garner D, Macaulay C, Palcic B. Malignancy associated changes in cervical smears: systematic changes in cytometric features with the grade of dysplasia. Anal Cell Pathol 1995; 9(3): 191-204.

[13]   Huisman A, Ploeger LS, Dullens HFJ, *et al*. Discrimination between benign and malignant prostate tissue using chromatin texture analysis in 3-D by confocal laser scanning microscopy. Prostate 2006; 67(3): 248-54.

[14]   Mommers EC, Poulin N, Meijer CJ, Baak JP, van Diest PJ. Malignancy-associated changes in breast tissue detected by image cytometry. Anal Cell Pathol 2000; 20(4): 187-95.

[15]   Poulin N, Susnik B, Guillaud M, Doudkine A, Worth A, Palcic B. Histometric texture analysis of DNA in thin sections from breast biopsies. Application to the detection of malignancy-associated changes in carcinoma in situ. Anal Quant Cytol Histol 1995; 17(5): 291-9.

[16]   Bartels PH, Montironi R, Hamilton PW, Thompson D, Vaught L, Bartels HG. Nuclear chromatin texture in prostatic lesions. I. PIN and adenocarcinoma. Anal Quant Cytol Histol 1998; 20(5): 389-96.

[17]   Bartels PH, Montironi R, Hamilton PW, Thompson D, Vaught L, Bartels HG. Nuclear chromatin texture in prostatic lesions. II. PIN and malignancy associated changes. Anal Quant Cytol Histol 1998; 20(5): 397-406.

[18]   Bartels PH, da Silva VD, Montironi R, *et al*. Chromatin texture signatures in nuclei from prostate lesions. Anal Quant Cytol Histol 1998; 20(5): 407-16.

[19]   Tekola P, Baak JP, van Ginkel HA, *et al*. Three-dimensional confocal laser scanning DNA ploidy cytometry in thick histological sections. J Pathol 1996; 180(2): 214-22.

[20]   Belien JA, van Ginkel AH, Tekola P, *et al*. Confocal DNA cytometry: a contour-based segmentation algorithm for automated three-dimensional image segmentation. Cytometry 2002; 49(1): 12-21.

[21]   Ploeger LS, Belien JA, Poulin NM, Grizzle W, van Diest PJ. Confocal 3D DNA cytometry: assessment of required coefficient of variation by computer simulation. Cell Oncol 2004; 26(3): 93-9.

[22]   Ploeger LS, Huisman A, van der GJ, *et al*. Implementation of accurate and fast DNA cytometry by confocal microscopy in 3D. Cell Oncol 2005; 27(4): 225-30.

[23]   Huisman A, Ploeger LS, Dullens HF, Poulin N, Grizzle WE, van Diest PJ. Development of 3D chromatin texture analysis using confocal laser scanning microscopy. Cell Oncol 2005; 27(5-6): 335-45.

[24]   Suzuki T, Fujikura K, Higashiyama T, Takata K. DNA staining for fluorescence and laser confocal microscopy. J Histochem Cytochem 1997;45(1): 49-53.

[25]   Doudkine A, Macaulay C, Poulin N, Palcic B. Nuclear texture measurements in image cytometry. Pathologica 1995; 87(3): 286-99.

[26]   Metzler V, Palm C, Lehmann T, Aach T. Texture Classification of Gray level Images by Multiscale Cross-Cooccurence Matrices. In: Conference on Pattern Recognition ICPR; Barcelona, Spain: IEEE Computer Society 2000; vol. 2: pp. 549-552.

[27]   Chaudhuri BB, Sarkar N. Texture segmentation using fractal dimension. IEEE Trans Pattern Anal Mach Intell 2005; 17(1): 72-7.

[28]   Markham J, Conchello JA. Artefacts in restored images due to intensity loss in three- dimensional fluorescence microscopy. J Microsc Oxford 2001; 204: 93-8.

[29]   Schrader M, Bahlmann K, Giese G, Hell SW. 4Pi-confocal imaging in fixed biological specimens. Biophys J 1998; 75(4): 1659-68.